NANO LETTERS

Letter

pubs.acs.org/NanoLett

Graphene Dynamic Synapse with Modulatable Plasticity

He Tian,[†,‡,⊥] Wentian Mi,[†,‡,⊥] Xue-Feng Wang,[†,‡] Haiming Zhao,[†,‡] Qian-Yi Xie,[†,‡] Cheng Li,[†,‡] Yu-Xing Li,[†,‡] Yi Yang,[†,‡] and Tian-Ling Ren*[,†,‡]

[†]Institute of Microelectronics, Tsinghua University, Beijing 100084, China

[‡]Tsinghua National Laboratory for Information Science and Technology (TNList), Tsinghua University, Beijing 100084, China

Supporting Information

ABSTRACT: The synaptic activities in the nervous system is the basis of memory and learning behaviors, and the concept of biological synapse has also spurred the development of neuromorphic engineering. In recent years, the hardware implementation of the biological synapse has been achieved based on CMOS circuits, resistive switching memory, and field effect transistors with ionic dielectrics. However, the artificial synapse with regulatable plasticity has never been realized of the device level. Here, an artificial dynamic synapse based on twisted bilayer graphene is demonstrated with tunable plasticity. Due to the ambipolar conductance of graphene, both behaviors of the excitatory synapse and the inhibitory synapse could be realized in a single device. Moreover, the synaptic plasticity could also be modulated by tuning the carrier density of graphene. Because the artificial synapse here could be regulated and inverted via changing the bottom gate voltage, the whole process of synapse development could be imitated. Hence, this work would offer a broad new vista for the 2D material electronics and guide the innovation of neuro-electronics fundamentally.

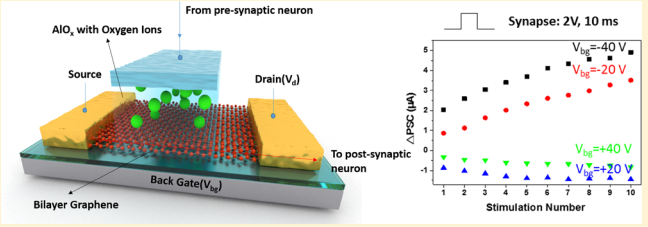

KEYWORDS: *graphene, nanoelectronics, neuromorphic device, artificial dynamic synapse, modulatable plasticity, spike-timing dependent plasticity*

There are quadrillions of synapses in the brain, and their firing patterns underwrite our consciousness, emotions, and behaviors.[1−3] The classical definition of a synapse is a specialized junction between two nerve cells, via which the signal from one nerve cell could be transmitted to another.[4] The synapse transmission efficiency is plastic and appears as the potentiation and depression of the synaptic strength in short or long-term. And the plasticity is the foundation of memory and learning behaviors. Because the nervous system based on synapses is a natural paradigm of high performance computation, lots of efforts have been made to achieve an artificial synapse with electronics[5−13] and even some artificial neural networks.[14,15]

However, only the static plasticity is not adequate to achieve the complex behaviors of a living organism. With the rapid progress of imaging technology, the dynamic movement in biological synapse has been discovered and has aroused widespread interest.[16,17] The dynamics of the synapse could be described at two levels. First, the ability of synapses to express plasticity is under regulation in the neural network.[18] The regulation insures that the plasticity is generated within a dynamic range and a proper period and, further, keeps the neural networks in the appropriate state for learning. (The detailed explanation is manifested in Supporting Information Section I.) Furthermore, the morphological changing of synapses is also an integral part of the physiological basis of learning mechanisms.[19] The synaptic morphological changing not only raises the abundance of synaptic plasticity but also holds possibilities for the self-healing and developing of the neural network.[20] All these dynamic features of synapses provide the infrastructure for highly complicated behaviors of living creatures. The variance of the synaptic plasticity is a considerable aspect of the dynamics. It not only provides a new path to understand the principle of neural networks but inspires the innovation in neuromorphic computation and artificial synaptic devices. Because most synaptic devices could only imitate the static plasticity, the dynamic synaptic device capable of plasticity modulation has yet to be realized and could mimic the behaviors of living organisms in higher dimensions and revolutionize the computation circuits.

To achieve the multilevel modulation of the artificial dynamic synapse, the transportation properties of the function material in the device should be easily modulated. As a remarkable material in various areas, graphene is highlighted for its great potential in biological applications.[21,22] Multitudes of excellent outcomes have been reported[23−26] that have indicated graphene as an ideal platform for bioelectronics. Here, we introduce graphene as the key material of realizing the artificial dynamic synapse due to its distinctive energy band structure and ambipolar conductance.[27] The conduction band and valence band of graphene overlaps at the Dirac point. The majority carriers could be switched between electrons and holes

Received: August 16, 2015
Revised: October 21, 2015
Published: October 26, 2015

DOI: 10.1021/acs.nanolett.5b03283
Nano Lett. 2015, 15, 8013−8019

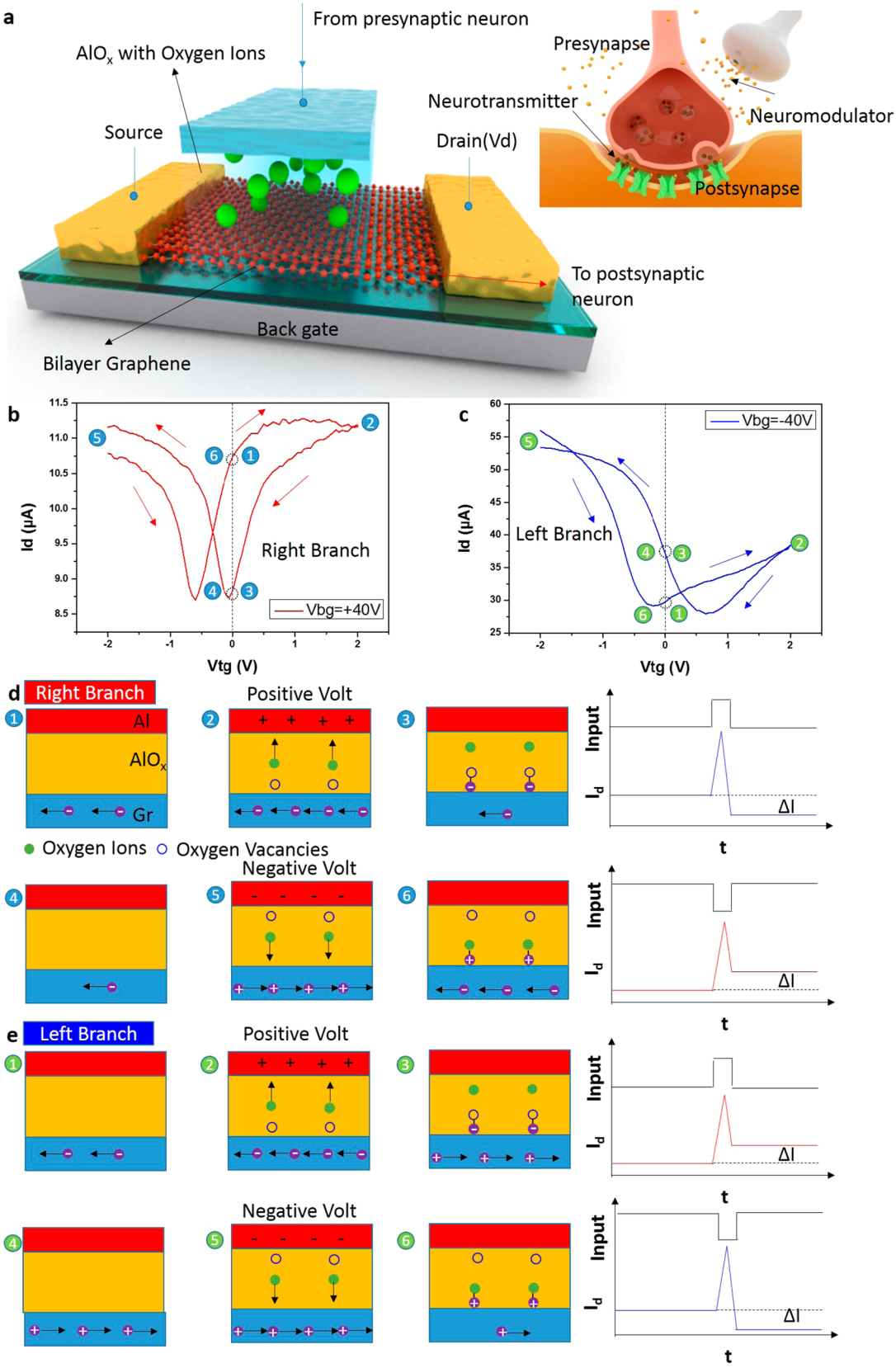

Figure 1. The graphene dynamic synapse (GDS). (a) Schematic of GDS. (b) I_d vs V_{tg} under the V_{bg} of +40 V with intersections on the right branch. (c) I_d vs V_{tg} under the V_{bg} of −40 V voltage with intersections on the left branch. The moving of the hysteresis curve reveals the working mechanisms of the (d) inhibitory synapse and (e) excitatory synapse, respectively.

by tuning the Fermi level, which matches the demand of artificial dynamic synapse precisely.

The plasticity is a basic function that needs to be realized in the artificial synapse. Here, the pairing of graphene and

DOI: 10.1021/acs.nanolett.5b03283
Nano Lett. 2015, 15, 8013−8019

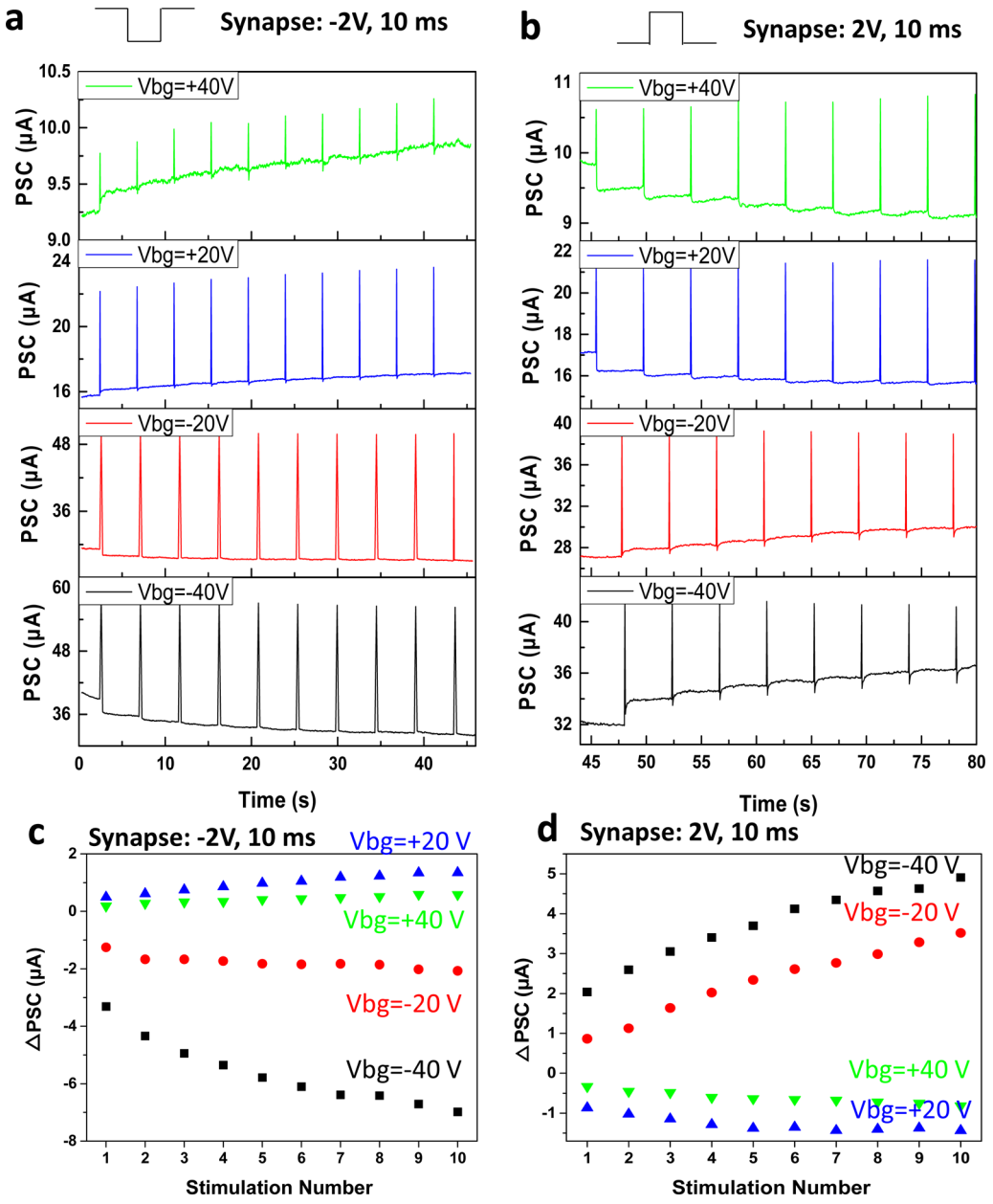

Figure 2. Modulation in graphene-based bionic dynamic synapse. The PSC with the (a) −2 V and (b) 2 V pulses under different V_{bg} (+40 V, + 20 V, −20 V, and −40 V). The ΔPSC with (c) −2 V and (d) 2 V pulses under different V_{bg} (+40 V, + 20 V, −20 V, and −40 V).

aluminum oxide is used as the function layers to imitate the synaptic plasticity. With different electrical fields applied, the defects in AlO_x would trap the carriers from graphene or release them, which could be reflected in the hysteresis curve when sweeping the applied voltage (see Supporting Information Section II).[28] Similarly, the current through graphene would be changed after a pulse is applied. And this is the basis of realizing the synaptic plasticity in the graphene device.

The schematic of the graphene dynamic synapse (GDS) is shown in Figure 1a (the lateral dimension of the device is presented in Supporting Information Section III), and the inset presents the structure of the biological synapse. An additional bottom gate was introduced in the GDS, which is key to realize modulatable plasticity. The graphene grown by chemical vapor deposition (CVD) is transferred to the highly doped Si substrate as bottom gate with 300 nm SiO_2. An Al electrode and two Au electrodes are patterned by electron-beam on top of the graphene as the top gate (1 μm width), source, and drain (the AFM image of the electrodes is presented in Supporting Information Figure S6). And a Al layer close to the graphene is oxidized to AlO_x as the dielectric (the fabrication process is presented in Supporting Information Section IV). With TEM combined with EDX, the thickness of the AlO_x is determined to be 5 nm and the Al/O ratio is ∼2.1. The input pulse applied on the top gate could alter the drain current and realize the plasticity. The constant voltage applied on the bottom gate would affect the carrier transportation in graphene and modulate the plasticity, thereby achieving the synaptic dynamics. To reveal the plasticity and synaptic dynamics simultaneously, the twisted bilayer graphene is used here.

Other kinds of graphene have been tested with the same structure. However, for monolayer graphene, some charges would be trapped by the SiO_2 defects and weaken the control of the bottom gate on the carriers (see Supporting Information

DOI: 10.1021/acs.nanolett.5b03283
Nano Lett. 2015, 15, 8013−8019

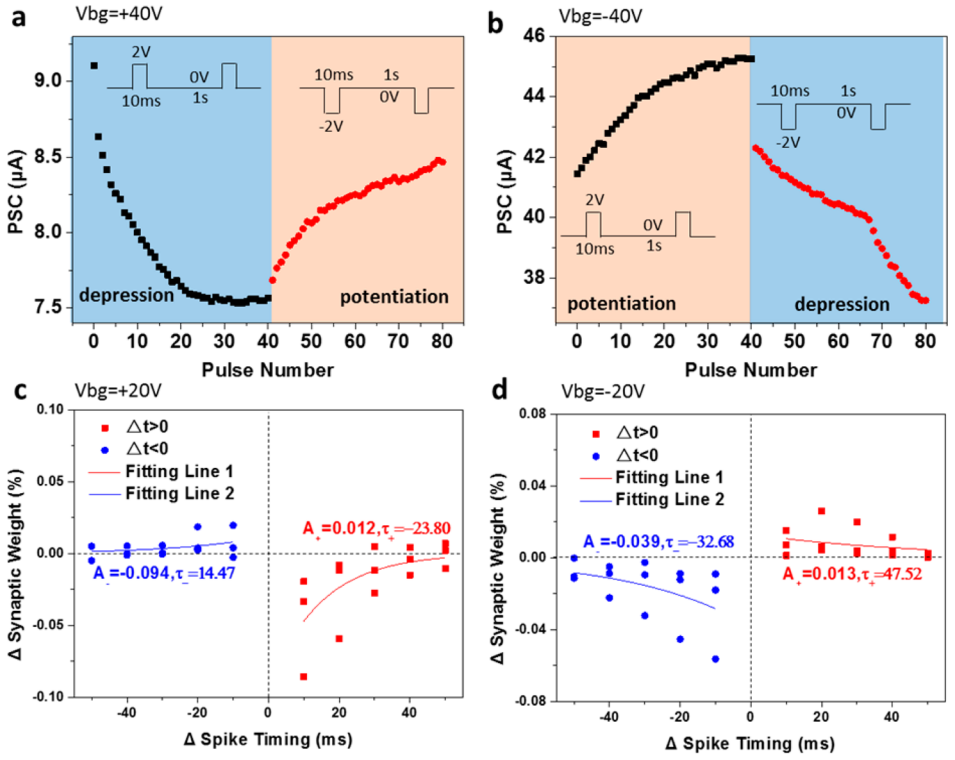

Figure 3. Rearrangement of synaptic properties. The long-term performance for (a) inhibitory synapse and (b) excitatory synapse. And the STDP performance for (c) inhibitory synapse and (d) excitatory synapse.

Section V). Disparate with the monolayer graphene, in twisted bilayer graphene, the two independent layers separate the effects of the two gates. Hence the overall shift of the hysteresis curve is easier compared to the monolayer graphene, which result in the intersection transfer between the two branches (Figure 1b,c) could only realize by the twisted bilayer graphene. (The simulation comparison of monolayer graphene and twisted bilayer graphene is shown in Supporting Information Section XIV.) Also, compared with the AB stacked graphene, the stacking with rotation guarantees that there is no band gap[29,30] complicating the influence mechanism of the current and depriving the synaptic behavior of the device (see Supporting Information Section VI). As for the trilayer graphene, the high carrier concentration would overwhelm the effect of gate modulation (see Supporting Information Section VII). Consequently, the twisted bilayer graphene is the optimal choice for the GDS.

Under a constant bottom gate voltage (V_{bg}) and a fixed drain voltage (0.1 V), an obvious hysteresis of drain current could be observed while sweeping the top gate voltage (V_{tg}) (Figure 1b and c). Here, the two parts on the different sides of the hysteresis curve are defined as left branch and right branch. Also, the arrows manifest the direction of the drain current (I_d) changing along with the V_{tg} sweeping. The voltage pulses are applied on the top gate as the input signal, generating a sudden increase of the drain current due to the great enhancement of the induced carrier and leading to the trapping or release of the carriers in graphene, which would result in the alteration of I_d. As the pulse could be regarded as a fast sweeping process, the type and density of the carriers before, during, and after the pulse is applied (the left, middle, and right columns in Figure 1d and e) could be reflected by the corresponding points on the hysteresis curve. Therefore, the amplitude and direction of ΔI_d could be manifested by the relative position of the two y-axis intersections of the hysteresis curve. Changing the V_{bg}, the carrier transportation could be also affected, presenting as the alteration of the y-axis intersection position on the hysteresis curve. For example, the intersections are on the right branch of the curve when V_{bg} = 40 V (Figure 1 b) and vice versa (Figure 1c). And this phenomenon is the key point to realize the modulatable synaptic plasticity, which is never realized in conventional synaptic devices (the comparison between the GDS and conventional synaptic devices is presented in Supporting Information Section VIII).

A similar process also occurs in a biological synapse, which is a junction between the presynapse neuron and the postsynapse neuron. The signal from the presynapse neuron, usually presented as a pulse, would be transmitted to the postsynapse neuron through the synapse and converted into the post synapse current (PSC). The value of the PSC corresponding to the same pulse is dependent on the previous activities in the synapse. This phenomenon is the concrete manifestation of the synaptic plasticity.[4] Here, the top gate, on which the voltage pulses are applied, counts as the presynapse neuron. And the graphene channel, through which the current (I_d) could be influenced by the top gate pulse, could be regarded as the postsynapse neuron, while the I_d here could be considered as the PSC. Moreover, the bottom gate, on which a voltage (V_{bg}) is applied to modulate the charge transportation in graphene in an independent dimension, provides a control terminal for imitating the dynamics of synapse.

To emulate synaptic behavior on the GDS, consecutive pulses (periodic 10 ms pulses spaced 4.3 s apart) of 2 and −2 V were applied on the top gate with a constant V_{bg}. The PSC of the GDS were altered gradually under the negative pulses (Figure 2a). And the positive pulses could also tune the PSC back to the initial state (Figure 2b). The result suggests that the static analogue synaptic plasticity could be realized in the GDS.

DOI: 10.1021/acs.nanolett.5b03283
Nano Lett. 2015, 15, 8013−8019

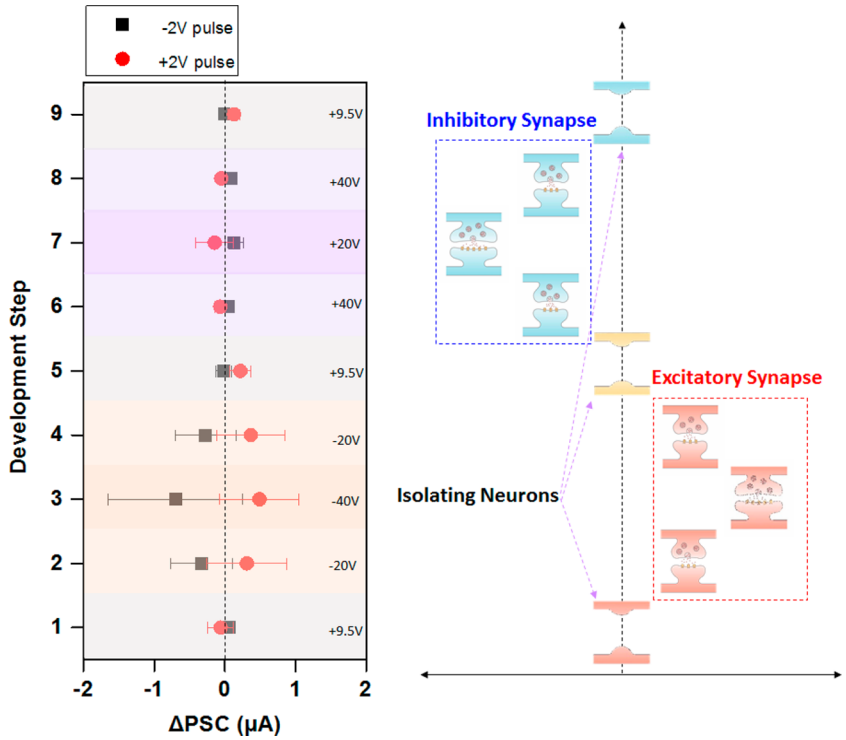

Figure 4. Development of synapse imitated by GDS. The left panel is the behavior mimicked by GDS by tuning the V_{bg}. The right panel is the corresponding steps of the synaptic developing. The step 1, 5, and 9 represent the isolating neurons. The step 2 to 4 and the step 6 to 8 represent the formation, maturation, and elimination of excitatory synapse and inhibitory synapse, respectively.

Changing the value of V_{bg}, the plasticity modulation could be also simulated. The variation of PSC after each pulse would be changed with different V_{bg} (−40 V, −20 V, + 20 V and +40 V) (Figure 2a and b). And the trend can be clearly shown in the diagram of the ΔPSC (Figure 2c and d), in which the ΔPSC after each pulse is recorded as a point. Turning the value of V_{bg} with unchanged sign (switch between −40 V and −20 V, or +20 V and +40 V), the value of ΔPSC would change significantly. However, since the graphene is vulnerable to be p-doped, the difference of ΔPSC when the V_{bg} varies in negative value (switching between −40 V and −20 V) is greater than the counterpart when the V_{bg} varies in positive value (switching between +40 V and +20 V). For the same reason, when V_{bg} rise from +20 V to +40 V, the I_d would get closer to the Dirac point on the I_d−V_{bg} curve (see Supporting Information Section IX), leading to the reducing of ΔPSC. As the ΔPSC is an indication of the synaptic plasticity, this phenomenon proves that the plasticity of the GDS can be excited or inhibited by turning the value of V_{bg}. Because the plasticity is modulated by a common bottom gate voltage, the modulatable synaptic plasticity of the artificial neural network could be achieved.

To characterize inversion of the synaptic plasticity clearly, the PSC with a long consecutive pulses series is shown in Figure 3a and b. Under a V_{bg} of +40 V, the PSC would decrease after positive pulses and increase after negative pulses (Figure 3a), which matches the behaviors of the inhibitory synapse in organisms. However, further turning the V_{bg} to −40 V, the positive pulses would lead to the increase of the PSC (Figure 3b), implying the inversion of the GDS to an excitatory synapse. The single pulse duration time property of the GDS has also been tested (see Supporting Information Section X), in which the altered PSC could last up to ∼300 s and the time constant of the current retrieving under different V_{tg} are almost the same. To give a further indication of the inversion, the spike-timing-dependent plasticity (STDP) function of the GDS under the V_{bg} of +20 V and −20 V are plotted (Figure 3c and d) and fit by the exponential function used in the biological STDP model. The STDP diagram suggests that the synaptic strength changes base on the relative timing of the input and output signal of the synapse, which could reflect the type of synapse obviously (the definition and measurement method are shown in Supporting Information Section XI, and the fitting process of STDP curve is shown in Supporting Information Section XII). All the points located in the second and fourth quadrants when the V_{bg} is +20 V, corresponding to the inhibitory synapse. However, under a V_{bg} of −20 V, the STDP function is limited in the first and third quadrants, corresponding to the excitatory synapse. The complementary STDP diagrams indicate the opposite behavior of the GDS after the same form of input when the sign of V_{bg} is different, which means the behavior of the GDS could be inversed by changing the sign of V_{bg}.

Because the widely modulatable plasticity could be achieved in the GDS, a relatively intact process of synapse development could be reproduced (Figure 4). The main steps of synapse development are usually considered to be formation, maturation, elimination, and remodeling.[18] The variation of plasticity, which is the important sign of the synaptic function, could be revealed by the GDS. When V_{bg} = +9.5 V, the GDS would not respond to the input pulses (see Supporting Information Section XIII), representing two isolating neurons without any synaptic connection. Turning the V_{bg} from +9.5 to +40 V, an inhibitory synapse could form between the two neurons. And the maturation of the synapse could be achieved by turning the V_{bg} from +40 to +20 V (the explanation for the current decrease is presented in Supporting Information

DOI: 10.1021/acs.nanolett.5b03283
Nano Lett. 2015, 15, 8013−8019

Section S11). Moreover, the synapse could be eliminated and reconstructed to excitatory synapse by changing the V_{bg} from positive to negative. The plasticity of both the inhibitory and excitatory synapses could be modulated by changing the value of V_{bg}. Hence, the GDS with higher dimensional dynamics could reveal the multilevel adjustability and reusability of the neuromorphic devices, which could boost the performance of synaptic computation exponentially.

In summary, a dynamic synaptic device was demonstrated based on twisted bilayer graphene, with the capability of nonvolatile analogue states and independent bottom gate modulation, which could mimic the multilevel dynamics of biological synapse. The lagging migration of a pulse-generated oxygen ions and vacancies in AlO_x would lead to the relatively sustainable alteration of the current through graphene, which resembles the plasticity of synapse. And the plasticity could be modulated by the additional bottom gate, which enables the GDS with the moudulatable plasticity. The back-gate structure is used to demonstrate the prototype of the GDS. Local back-gate technology has been reported and widely known as an efficient method to realize wafer-scale nano devices.[31] For an array of GDS, local back-gate technology also can be used in the future to realize the individual back-gate control on each GDS. Such innovative graphene dynamic synaptic devices would introduce a novel material system for the artificial neural network and be applied to block the neuromorphic system capable of autonomous learning and self-healing abilities.

Methods. *Graphene Growth and Transfer.* Large hexagonal single-crystal few layer graphene grains were grown by atmospheric pressure CVD of Ar-diluted methane (80 ppm) on 10 μm thick polycrystalline Cu foils. Prior to growth, the Cu foils were cleaned with acetone and IPA, followed by etching in acetic acid for 30 min to remove surface oxides. The Cu foils were then mounted in the CVD chamber and the furnace was heated to 1050 °C over 30 min, with constant flows of 300 sccm Ar and 15 sccm H_2. After reaching 1050 °C, the Cu foils were annealed for 150 min without changing the gas flow. For graphene growth, 150 sccm methane mixed with the flows of 150 sccm Ar and of 15 sccm H_2 was fed into the reaction chamber for 60 min to form monolayer graphene, bilayer graphene (twist and AB stacking), and ABA stacking trilayer graphene. Following the growth, the Cu foils were moved to the cooling zone under the protection of Ar and H_2. For the transfer process, the graphene sheets were first coated with a thin layer of PMMA, followed by etching in HCl aqueous solution to remove the Cu. Then, the PMMA film, along with the attached graphene, was transferred onto a silicon substrate. Finally, the PMMA was removed using acetone and IPA.

Device Fabrication. GDS was made with e-beam lithography (EBL) and standard lift-off processes. First, the device region was isolated using O_2 plasma. A 60 nm thick layer of Al was deposited by thermal evaporation and the substrate was encapsulated in a sealed chamber filled with high purity oxygen (>99.999%) at a pressure of 2 kg/cm^2. External source/drain electrodes were made of Cr/Au (0.5/60 nm). Finally, after 24 h exposure, the Al electrodes were surrounded with a continuous ultrathin AlO_x, which acted as the dielectric. For each EBL step, PMMA was spin-coated on the graphene film, followed by baking at 130 °C for 30 min. The exposed PMMA was developed with methyl isobutyl ketone (MIBK) and IPA in the ratio of 3:8. The EBL was carried out using a scanning electron microscope (JSM-840A) equipped with an e-beam writer (Raith Elphy Quantum).

Electrical Measurements. Electrical performance of GDS is measured by probe station (Keithley 4200). Presynaptic spikes are applied on the top gate electrode, and the pulse width is 10 ms.

■ ASSOCIATED CONTENT

Supporting Information

The Supporting Information is available free of charge on the ACS Publications website at DOI: 10.1021/acs.nanolett.5b03283.

Testing results and discussion of GDS. (PDF)

■ AUTHOR INFORMATION

Corresponding Author

*E-mail: RenTL@tsinghua.edu.cn.

Author Contributions

⊥H.T. and W.M: These authors contributed equally to this work.

Notes

The authors declare no competing financial interest.

■ ACKNOWLEDGMENTS

We would like to thank Prof. Po-Wen Chiu from National Tsing Hua University for the valuable suggestions on material preparation and device fabrication. And we appreciate Prof. Qing Wan from Nanjing University for helping set up the test environment. This work was supported by National Natural Science Foundation of China (61574083, 61434001), National Basic Research Program of China (973 Program, 2015CB352100), National Key Project of Science and Technology (2011ZX02403-002), and Special Fund for Agro-scientific Research in the Public Interest (201303107) of China.

■ REFERENCES

(1) Churchland, M. M.; Cunningham, J. P.; Kaufman, M. T.; Foster, J. D.; Nuyujukian, P.; Ryu, S. I.; Shenoy, K. V. *Nature* **2012**, *487* (7405), 51−6.

(2) Lisman, J. *Proc. Natl. Acad. Sci. U. S. A.* **1989**, *86* (23), 9574−8.

(3) Wen, Z.; Nguyen, H. N.; Guo, Z.; Lalli, M. A.; Wang, X.; Su, Y.; Kim, N. S.; Yoon, K. J.; Shin, J.; Zhang, C.; Makri, G.; Nauen, D.; Yu, H.; Guzman, E.; Chiang, C. H.; Yoritomo, N.; Kaibuchi, K.; Zou, J.; Christian, K. M.; Cheng, L.; Ross, C. A.; Margolis, R. L.; Chen, G.; Kosik, K. S.; Song, H.; Ming, G. L. *Nature* **2014**, *515*, 414.

(4) Sherrington, C. S. *The integrative action of the nervous system: Silliman memorial lecture*; Yale University Press: New Haven, CT, 1906.

(5) Watanabe, T.; Kimura, K.; Aoki, M.; Sakata, T.; Ito, K. *Neural Networks, IEEE Transactions on* **1993**, *4* (3), 387−393.

(6) Snider, G. S. Spike-timing-dependent learning in memristive nanodevices. *IEEE Symp. Nanoscale Archit.* **2008**, 85−92, DOI: 10.1109/NANOARCH.2008.4585796.

(7) Jo, S. H.; Chang, T.; Ebong, I.; Bhadviya, B. B.; Mazumder, P.; Lu, W. *Nano Lett.* **2010**, *10* (4), 1297−301.

(8) Ohno, T.; Hasegawa, T.; Tsuruoka, T.; Terabe, K.; Gimzewski, J. K.; Aono, M. *Nat. Mater.* **2011**, *10* (8), 591−5.

(9) Yu, S.; Wu, Y.; Jeyasingh, R.; Kuzum, D.; Wong, H.-S. *IEEE Trans. Electron Devices* **2011**, *58* (8), 2729−2737.

(10) Kim, K.; Chen, C. L.; Truong, Q.; Shen, A. M.; Chen, Y. *Adv. Mater.* **2013**, *25* (12), 1693−8.

(11) Shi, J.; Ha, S. D.; Zhou, Y.; Schoofs, F.; Ramanathan, S. *Nat. Commun.* **2013**, *4*, 2676.

(12) Yu, S.; Gao, B.; Fang, Z.; Yu, H.; Kang, J.; Wong, H. S. *Adv. Mater.* **2013**, *25* (12), 1774−9.

DOI: 10.1021/acs.nanolett.5b03283
Nano Lett. 2015, 15, 8013−8019

(13) Zhu, L. Q.; Wan, C. J.; Guo, L. Q.; Shi, Y.; Wan, Q. *Nat. Commun.* **2014**, *5*, 3158.
(14) Kim, K.; Tudor, A.; Chen, C.-L.; Lee, D.; Shen, A. M.; Chen, Y. *J. Compos. Mater.* **2015**, *49*, 1809−1822.
(15) Shen, A. M.; Kim, K.; Tudor, A.; Lee, D.; Chen, Y. *Small* **2015**, *11* (13), 1571−1579.
(16) Meyer, A. C.; Frank, T.; Khimich, D.; Hoch, G.; Riedel, D.; Chapochnikov, N. M.; Yarin, Y. M.; Harke, B.; Hell, S. W.; Egner, A.; Moser, T. *Nat. Neurosci.* **2009**, *12* (4), 444−53.
(17) Cohen-Cory, S. *Science* **2002**, *298* (5594), 770−6.
(18) Abraham, W. C. *Nat. Rev. Neurosci.* **2008**, *9* (5), 387.
(19) De Roo, M.; Klauser, P.; Garcia, P. M.; Poglia, L.; Muller, D. Spine dynamics and synapse remodeling during LTP and memory processes. In *Progress in Brain Research*; Wayne, S. Sossin, J.-C. L. V, F. C., Sylvie, B., Eds.; Elsevier: Amsterdam, 2008; Chapter 11, Vol. *169*, pp 199−207.
(20) Fourgeaud, L.; Boulanger, L. M. *Cell* **2007**, *131* (6), 1034−6.
(21) Kostarelos, K.; Novoselov, K. S. *Nat. Nanotechnol.* **2014**, *9* (10), 744−745.
(22) Siwy, Z. S.; Davenport, M. *Nat. Nanotechnol.* **2010**, *5* (10), 697−698.
(23) Garaj, S.; Hubbard, W.; Reina, A.; Kong, J.; Branton, D.; Golovchenko, J. *Nature* **2010**, *467* (7312), 190−193.
(24) Yang, K.; Zhang, S.; Zhang, G.; Sun, X.; Lee, S.-T.; Liu, Z. *Nano Lett.* **2010**, *10* (9), 3318−3323.
(25) Singh, S. K.; Singh, M. K.; Kulkarni, P. P.; Sonkar, V. K.; Grácio, J. J.; Dash, D. *ACS Nano* **2012**, *6* (3), 2731−2740.
(26) Patil, A. J.; Vickery, J. L.; Scott, T. B.; Mann, S. *Adv. Mater.* **2009**, *21* (31), 3159−3164.
(27) Heersche, H. B.; Jarillo-Herrero, P.; Oostinga, J. B.; Vandersypen, L. M.; Morpurgo, A. F. *Nature* **2007**, *446* (7131), 56−59.
(28) Wang, H.; Wu, Y.; Cong, C.; Shang, J.; Yu, T. *ACS Nano* **2010**, *4* (12), 7221−7228.
(29) Dos Santos, J. L.; Peres, N.; Neto, A. C. *Phys. Rev. Lett.* **2007**, *99* (25), 256802.
(30) Kim, K. S.; Walter, A. L.; Moreschini, L.; Seyller, T.; Horn, K.; Rotenberg, E.; Bostwick, A. *Nat. Mater.* **2013**, *12* (10), 887−892.
(31) Shulaker, M. M.; Hills, G.; Patil, N.; Wei, H.; Chen, H.-Y.; Wong, H.-S. P.; Mitra, S. *Nature* **2013**, *501* (7468), 526−530.

DOI: 10.1021/acs.nanolett.5b03283
Nano Lett. 2015, 15, 8013−8019